論文 / 著書情報
Article / Book Information

Title	A new performance index of LQR for combination of passive base isolation and active structural control
Authors	Kou Miyamoto, Daiki Sato, Jinhua She
Citation	Engineering Structures, Vol. 157, pp. 280-299
Pub. date	2018, 2
DOI	http://dx.doi.org/10.1016/j.engstruct.2017.11.070
Creative Commons	See next page.
Note	This file is author (final) version.

License

A new performance index of LQR for combination of passive base isolation and active structural control

Kou Miyamoto[a], Daiki Sato[b,*], Jinhua She[c]

[a]*School of Environment and Society, Architecture and Building Engineering, Tokyo Institute of Technology, Yokohama, Kanagawa 226-8503, Japan*
[b]*Laboratory for Future Interdisciplinary Research of Science and Technology (FIRST), Tokyo Institute of Technology, Yokohama, Kanagawa 226-8503, Japan*
[c]*School of Engineering, Tokyo University of Technology, Hachioji, Tokyo 192-0982, Japan*

Abstract

This paper considers the problem of designing a state-feedback controller with both passive base isolation (PBI) and active structural control (ASC). In order to improve control performance, state-feedback gains are designed based on the linear quadratic regulator (LQR) method that optimizes a new performance index containing absolute acceleration, and inter-story drifts and velocity. Simulations on a model of an eleven degree-of-freedom shear building for four earthquake accelerograms are used to verify this method. Comparison studies show that, compared with PBI, the combination of PBI and ASC improves control performance; and this method yields better control results than the conventional ASC, which considers relative displacement and relative velocity of each story. The results are also discussed from the viewpoint of control system structure regarding the location of system zeros. In addition, the effect of weights in the LQR on control performance is discussed. A method for selecting the weights is presented by using the infinity norm of a system as a criterion to visualize their effect.

Keywords: Active structural control (ASC), Linear-quadratic regulator (LQR), Absolute acceleration, Inter-story drift, Passive base isolation (PBI), Seismic vibration, Unstable zero, Vibration reduction.

1. Introduction

Passive base isolation (PBI) installed in buildings not only suppresses vibrations, but also ensures safe use of the buildings after earthquakes [1, 2]. The Kobe earthquake on January 17, 1995 triggered a demand for PBI in Japan, and the number of passive-base-isolated high-rise buildings has been steadily increasing in the last two decades [3].

A new base isolation system called a rubber-layer rolling bearing was presented in [4, 5].

As the installation of PBI enlarges the natural period of a building, it results in a reduction in the absolute acceleration of buildings. However, it increases displacement of the PBI story and may force it beyond its allowable range.

Some aluminum or steel devices were also used as passive energy dissipating systems for a building to suppress the displacement [6, 7, 8]. If a building employs these kinds of devices, its stiffness increases and the natural period becomes short. This may increases the absolute acceleration of the building.

Active structural control (ASC) is a strategy for vibration reduction that incorporates control engineering and civil engineering. The first full-scale ASC in the world was installed in the Kyobashi Center Building in 1989 in Japan. Studies in this field have been showing rapid progress since then, and ASC is now widely used in civil structures all over the world [9, 10].

The linear-quadratic regulator (LQR) is one of the most commonly used design methods in control theory. It designs a state-feedback gain by minimizing a performance index that considers the weighted state and control input of a plant. This method has been used in the design of ASC and semi-active structural control systems. Loh at el. conducted an experiment using a real-scale active tendon to demonstrate the validity of ASC [11].

The selection of a performance index for the LQR is a key to designing a satisfactory ASC system. While most studies selected relative displacement and velocity of each story [12, 13, 14, 15], some studies considered kinetic energy [16, 17], inter-story drifts [18, 19], or absolute acceleration [19, 20]. In the structural control of a building, suppressing inter-story drifts prevents the exfoliation of exterior materials and the plastic behavior of a building. On the other hand, suppressing absolute acceleration not only protects a building by reducing story shear-force from an earthquake, but also protects people and property by preventing things such as furniture and equipment inside the facility from falling. Thus, it is important to build a performance index that considers the inter-story drifts, the relative velocity, and the absolute acceleration of all stories of a building for the design of a practical ASC system. A new performance index that contains those items is presented in this paper.

The method utilized to weights to integrate evaluation items in a performance index is also an important issue for system design. However, only few attempts have so far been made to accomplish it such methods. Most studies selected weights rather

*Corresponding author. Tel. & Fax: +81-45(924)5306. *E-mail address:* sato.d.aa@m.titech.ac.jp (D. Sato)

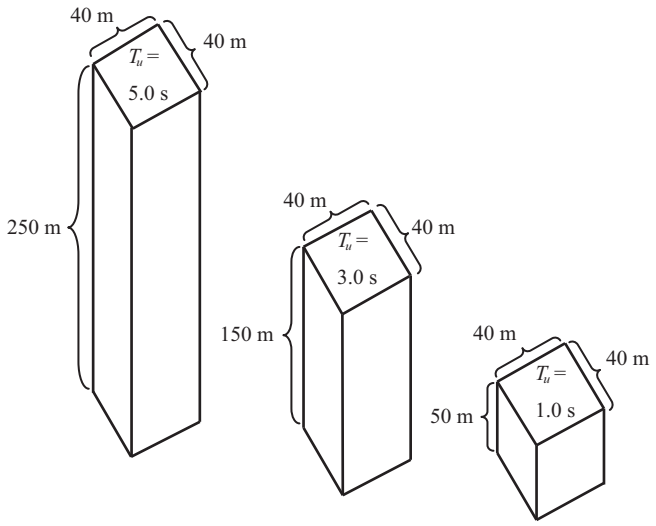

Fig. 1: Models of structures.

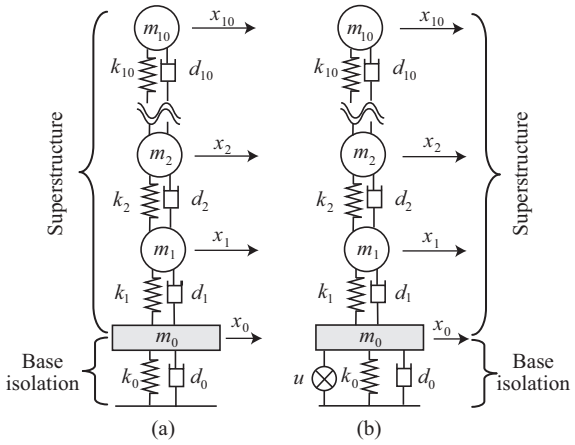

Fig. 2: 11-DOF model of [(a) NC and (b) LQR or AD-LQR].

subjectively and determined them by trial and error [12]. Regarding this issue in structural control, a study examined the effect of different weights for a single-degree-of-freedom system [21]. However, buildings are usually multi-degree-of-freedom (MDOF) systems. Therefore, it is of practical value to investigate weight selection for an MDOF system.

PBI enlarges the natural period. This may result in a large displacement. On the other hand, ASC generally increases the apparent stiffness of a building by suppressing the displacement. It shortens the apparent natural period, and may cause a large absolute acceleration. Thus, a good combination of PBI and ASC provides satisfactory structural control performance with small control energy. Focusing on this characteristic, this paper considers the problem of structural control using the combination of PBI and ASC for high-rise buildings. A new performance index is used to design a suitable ASC system. The superiority of the method over PBI or conventional ASC is demonstrated through simulations, and the analysis of control inputs and the control system structure.

In this paper, I is an identity matrix with appropriate dimension. For simplicity, a system only with PBI is called NC (no control); a conventional ASC system that minimizes the displacement and velocity of each story is called a conventional LQR; and an ASC system that minimizes the absolute acceleration, and inter-story drift and velocity of each story presented in this paper is called AD-LQR for short.

2. Structures and base-isolation models

This study used three building models with heights of 250 m, 150 m, and 50 m. The floor areas of the models were all 40 m × 40 m (Fig. 1). Each was described as a 10-DOF shear building model (Fig. 2). PBI was installed under the structure. The ASC device was located at the PBI story. Thus, the models have 11 DOFs (10 DOFs for the superstructure and 1 DOF for the base isolation).

The parameters are as follows (Fig. 1):

Mass per unit area of base isolation: 2551 kg/m^2

Damping for period of PBI (ζ_b)**:** 0.05

Damping of superstructure: stiffness-proportional damping model (the damping ratio for the first mode, ζ_u, is assumed to be 0.02)

Natural periods of superstructure of first mode (T_u)**:** 1.0 s for the 50-m-high building, 3.0 s for the 150-m-high building, and 5.0 s for the 250-m-high building

Density of superstructure (for all floors): 175 kg/m^3

Height of superstructure (h_u)**:** $= T_u/0.02$ m

Stiffness of the i-th story of superstructure [22]:

$$\begin{cases} k_i = \dfrac{\omega^2 m_i \phi_i + k_{i+1}(\phi_{i+1} - \phi_i)}{\phi_i - \phi_{i-1}},\ i = 2, \ldots, 9, \\ k_1 = \dfrac{\omega^2 m_1 \phi_1 + k_2(\phi_2 - \phi_1)}{\phi_1},\ k_{10} = \dfrac{\omega^2 m_{10} \phi_{10}}{\phi_{10} - \phi_9}, \end{cases} \tag{1}$$

where ω is the first natural circular frequency; and for the i-th story ($i = 1, 2, \ldots, 10$), ϕ_i is the first natural mode, and m_i is the mass.

To use the LQR method, which is a linear control strategy [27], the laminated rubber in the PBI is modeled as a linear spring (Fig. 3), and the viscous damper in the PBI is modeled as a linear dashpot (Fig. 4). The stiffness, k_0, and the damping coefficient, d_0, of the PBI are given by

$$k_0 = \frac{4\pi^2(m_u + m_0)}{T_0^2},\ d_0 = 2\zeta_b \sqrt{(m_u + m_0)k_0}, \tag{2}$$

respectively, where m_u is the total mass of the superstructure; and m_0 is given by the product of the density of the base and the floor area.

Let T_0 be the period of the PBI with the superstructure being assumed to be a rigid body. The combinations of the parameters of buildings (Table 1) are used to verify the validity of the method presented in this paper and to perform a comparison with other methods. In the table, T is the period of the first mode of the building with the base isolation.

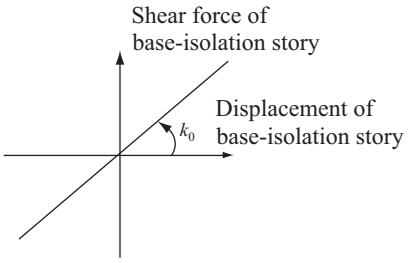

Fig. 3: Linear spring model of laminated rubber.

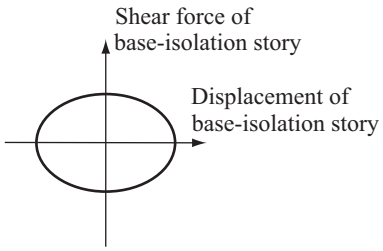

Fig. 4: Linear dashpot model of linear viscous damper.

3. Design of LQR controllers

The dynamics of an 11-DOF building with an ASC device and the PBI are described by

$$M\ddot{x}(t) + D\dot{x}(t) + Kx(t) = -ME\ddot{x}_g(t) + E_u u(t), \tag{3}$$

where

$$M = \begin{bmatrix} m_0 & & & & 0 \\ & m_1 & & & \\ & & m_2 & & \\ 0 & & & \ddots & \\ & & & & m_{10} \end{bmatrix},$$

$$D = \begin{bmatrix} d_0 + d_1 & -d_1 & & & 0 \\ -d_1 & d_1 + d_2 & -d_2 & & \\ & -d_2 & d_2 + d_3 & -d_3 & \\ & & & \ddots & \\ 0 & & & & d_{10} \end{bmatrix},$$

$$K = \begin{bmatrix} k_0 + k_1 & -k_1 & & & 0 \\ -k_1 & k_1 + k_2 & -k_2 & & \\ & -k_2 & k_2 + k_3 & -k_3 & \\ & & & \ddots & \\ 0 & & & & k_{10} \end{bmatrix},$$

$$E = \begin{bmatrix} 1 & 1 & 1 & \cdots & 1 \end{bmatrix}^{\mathrm{T}},$$

$$E_u = \begin{bmatrix} 1 & 0 & 0 & \cdots & 0 \end{bmatrix}^{\mathrm{T}}.$$

The variables are defined as follows:

$x(t)$**:** relative displacement vector of stories (= $[x_0(t),\ x_1(t),\ \ldots,\ x_{10}(t)]^{\mathrm{T}}$)

$u(t)$**:** control input produced by actuator

Table 1: Combinations of T_u, T, T_0, and ζ_b for verification.

T_u [s]	T_0 [s]	T [s]	ζ_b
1.0	2.0	2.2	0.05
	4.0	4.1	
3.0	4.0	4.8	
	6.0	6.6	
5.0	6.0	7.6	
	8.0	9.2	

$\ddot{x}_g(t)$**:** ground acceleration

M**:** mass matrix

D**:** damping matrix

K**:** stiffness matrix.

Note that the dynamics of the building without PBI have the same structure, and we just need to remove the row and column corresponding to the base story (the parameters m_0, d_0, and k_0). The state-space expression of (3) is

$$\begin{cases} \dot{\chi}(t) = A\chi(t) + B_u u(t) + B_d \ddot{x}_g(t), \\ y(t) = C\chi(t), \end{cases} \tag{4}$$

where

$$\begin{cases} \chi(t) = \begin{bmatrix} x(t) \\ \dot{x}(t) \end{bmatrix}, \\ A = \begin{bmatrix} 0 & I \\ -M^{-1}K & -M^{-1}D \end{bmatrix}, \\ B_u = \begin{bmatrix} 0 \\ -M^{-1}E_u \end{bmatrix},\ B_d = \begin{bmatrix} 0 \\ -E \end{bmatrix}, \end{cases}$$

and A is the system matrix determining the dynamic characteristics of the plant, B_u is the control-input matrix indicating the placement of the ASC device, B_d is the disturbance-input matrix indicating the places that the disturbance is added, and C is the output matrix showing the placement of sensors. If all states are available, then C can be chosen to be an identity matrix.

The feedback control law

$$u(t) = K_p\chi(t) \tag{5}$$

is used, where K_p is the state-feedback gain that is designed using the LQR method. The block diagram of the control system is shown in Fig. 5. Conventional ASC systems find a state-feedback gain by minimizing the following performance index [12]

$$J_c = \int_0^\infty \left\{\chi^{\mathrm{T}}(t)Q_c\chi(t) + u^{\mathrm{T}}(t)R_c u(t)\right\} dt. \tag{6}$$

It takes account of the relative displacement and velocity of each story. In (6), Q_c (> 0) and R_c (> 0) are weights for the state and control input, respectively. A big diagonal entry in Q_c results in a feedback gain that suppresses the corresponding state, and increasing R_c suppresses the control input.

The inter-story drift angles are

$$\theta_i = \arctan\frac{x_i - x_{i-1}}{h_i} \approx \frac{x_i - x_{i-1}}{h_i}, i = 1, 2, \ldots, 10, \tag{7}$$

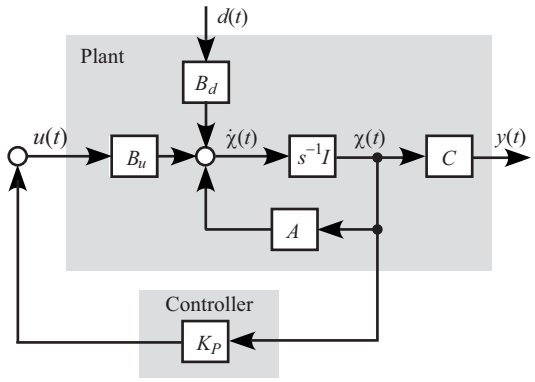

Fig. 5: Block diagram of ASC.

where h_i is the height of each story. Clearly, the inter-story drift angles are the same for the inter-story drifts except for the scaling factor $1/h_i$. Note that inter-story drifts and absolute acceleration have not been considered for most ASC systems. However, suppressing those two kinds of variables in a small range not only reduces damage of buildings, but also protects people from earthquakes. Thus, evaluating these two items is of importance in ASC. This study considered a new performance index

$$\begin{aligned} J = \int_0^\infty \Big\{ & \begin{bmatrix} \Delta x^{\mathrm{T}}(t) & \Delta \dot{x}^{\mathrm{T}}(t) \end{bmatrix} Q_d \begin{bmatrix} \Delta x(t) \\ \Delta \dot{x}(t) \end{bmatrix} \\ & + \left[\ddot{x}(t) + E\ddot{x}_g(t) \right]^{\mathrm{T}} Q_g \left[\ddot{x}(t) + E\ddot{x}_g(t) \right] \\ & + u^{\mathrm{T}}(t) R_u u(t) \Big\} dt, \end{aligned} \tag{8}$$

where Q_d (> 0), Q_g (> 0), and R_u (> 0). While the conventional LQR considers the relative displacement and the relative velocity of each story, the AD-LQR considers the absolute acceleration, and the inter-story drifts and velocity.

In (8), the vector of the inter-story drifts is given by

$$\begin{cases} \Delta x(t) = \begin{bmatrix} \Delta x_0(t) & \Delta x_1(t) & \cdots & \Delta x_{10}(t) \end{bmatrix}^{\mathrm{T}}, \\ \Delta x_i(t) = \begin{cases} x_0(t), & i = 0, \\ x_i(t) - x_{i-1}(t), & i = 1, \ldots, 10, \end{cases} \end{cases} \tag{9}$$

where $i = 0$ means the PBI story, and i from 1 to 10 means the stories of the superstructure.

There exists a nonsingular matrix Υ and W that ensure

$$\begin{cases} W \begin{bmatrix} \Delta x(t) \\ \Delta \dot{x}(t) \end{bmatrix} = \begin{bmatrix} \Upsilon & 0 \\ 0 & \Upsilon \end{bmatrix} \begin{bmatrix} \Delta x(t) \\ \Delta \dot{x}(t) \end{bmatrix} = \chi(t), \\ \Upsilon = \begin{bmatrix} 1 & & & 0 \\ 1 & 1 & & \\ & & \ddots & \\ 1 & 1 & \cdots & 1 \end{bmatrix}. \end{cases} \tag{10}$$

Rewriting (3) yields

$$\ddot{x}(t) + E\ddot{x}_g(t) = \Xi\chi(t) + \Psi u(t) \tag{11}$$

where

$$\Xi = \begin{bmatrix} -M^{-1}K & -M^{-1} \end{bmatrix}, \ \Psi = -M^{-1}E_u.$$

Substituting (11) into (8) gives

$$J = \int_0^\infty \left\{ \chi^{\mathrm{T}}(t) Q \chi(t) + 2\chi^{\mathrm{T}}(t) H u(t) + u^{\mathrm{T}}(t) R u(t) \right\} dt, \tag{12}$$

where

$$\begin{cases} Q = W^{-\mathrm{T}} Q_d W^{-1} + \Xi^{\mathrm{T}} Q_g \Xi, \\ H = -\Xi^{\mathrm{T}} Q_g \Psi + \Psi^{\mathrm{T}} Q_g \Xi, \\ R = \Psi_u^{\mathrm{T}} Q_g \Psi + R_u. \end{cases} \tag{13}$$

Note that, unlike the standard performance index (6) used in many ASC systems, the index (12) contains a cross term of $\chi(t)$ and $u(t)$. Optimizing (12) yields a state-feedback gain [12]

$$K_p = -R^{-1}(S^{\mathrm{T}} + B_u^{\mathrm{T}} P), \tag{14}$$

where P is a positive symmetrical solution of the following Riccati equation

$$\begin{aligned} & \left(A - B_u R^{-1} S^{\mathrm{T}} \right)^{\mathrm{T}} P + P \left(A - B_u R^{-1} S^{\mathrm{T}} \right) \\ & \quad + Q - P B_u R^{-1} B_u^{\mathrm{T}} P - S R^{-1} S^{\mathrm{T}} = 0. \end{aligned} \tag{15}$$

If the Riccati equation, (14), is solvable, then the feedback system matrix $A - B_u K_p$ is stable for the state-feedback gain K_p given by (14).

4. Numerical verification

This section uses numerical examples to demonstrate the validity of the AD-LQR, and shows its superiority over the PBI and LQRs 1-3 method.

4.1. Earthquake waves

Two artificial earthquake waves were used in this study. They were reproduced from real earthquake waves that minimized the effects of natural periods of the original waves:

1. Art Hachinohe wave: the spectrum of the pseudovelocity response, ${}_pS_v$, is 100 cm/s for a building with damping ratio of 5% after a corner period of 0.64 s, and the phase characteristic is the same as the earthquake wave of the 1968 Hachinohe EW.
2. Art Kobe wave: the spectrum of the pseudovelocity response, ${}_pS_v$, is 100 cm/s for a building with damping ratio of 5% after a corner period of 0.64 s, and the phase characteristic is the same as the earthquake wave of the 1995 JMS Kobe NS.
3. El-Centro wave: El-Centro earthquake NS 1940.
4. Tokachi wave: Tokachi-oki earthquake NS 1968.

The accelerograms and the spectrums of the pseudovelocity responses of these four waves are shown in Figs. 6-9.

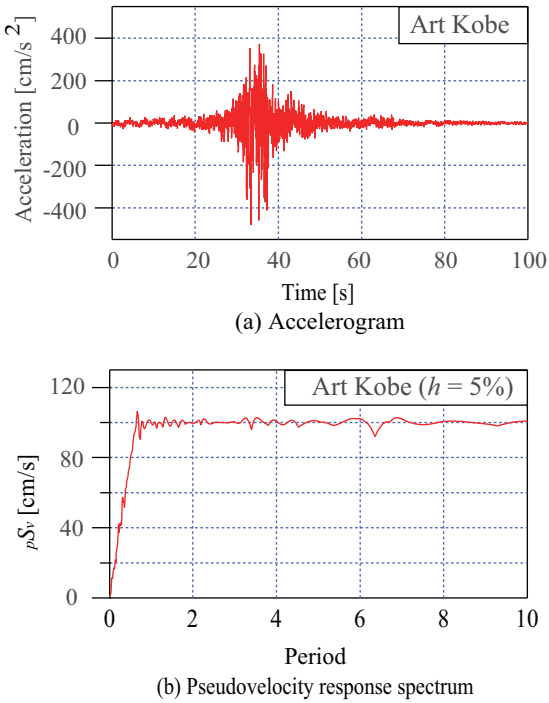

Fig. 6: Art Kobe wave [(a) Accelerogram and (b) Pseudovelocity response spectrum for damping ratio of 5%].

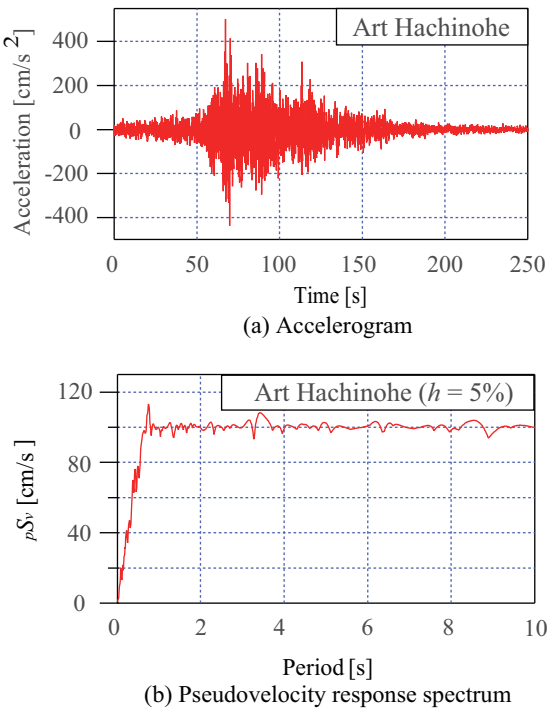

Fig. 7: Art Hachinohe wave [(a) Accelerogram and (b) Pseudovelocity response spectrum for damping ratio of 5%].

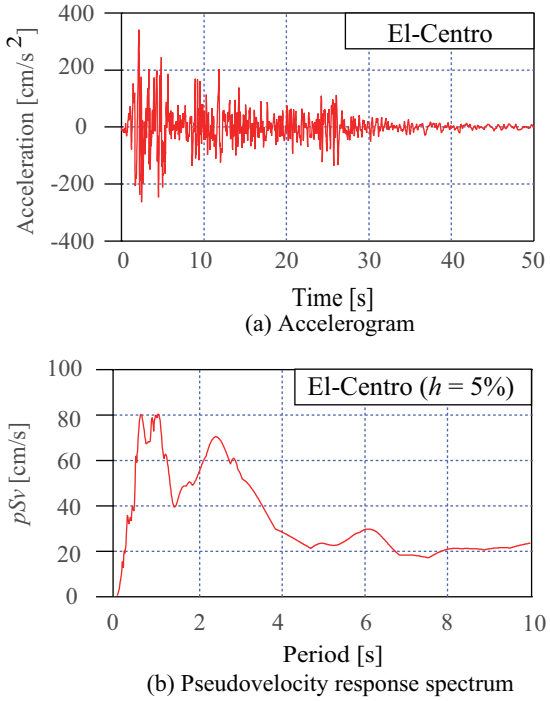

Fig. 8: El-Centro wave [(a) Accelerogram and (b) Pseudovelocity response spectrum for damping ratio of 5%].

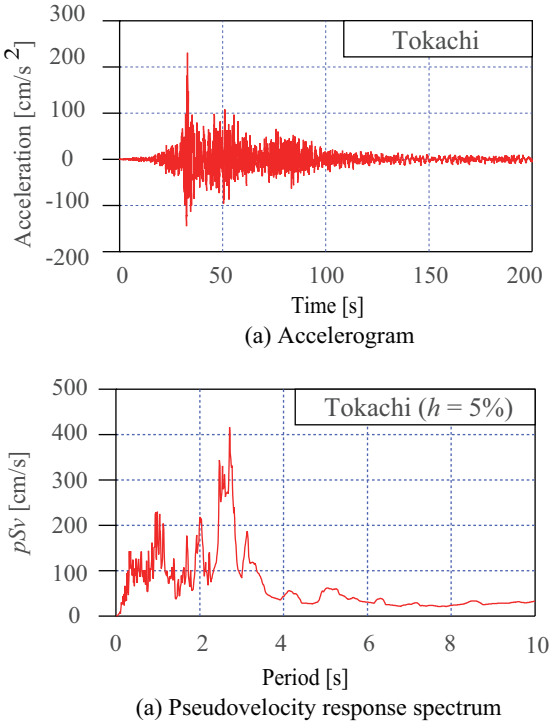

Fig. 9: Tokachi wave [(a) Accelerogram and (b) Pseudovelocity response spectrum for damping ratio of 5%].

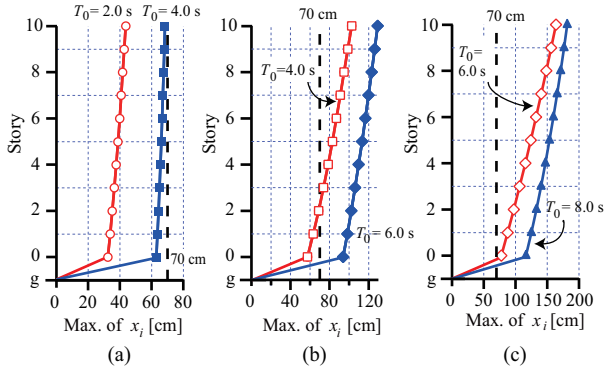

Fig. 10: Maximum displacement of NC for Art Kobe wave [(a) T_u = 1.0 s, (b) T_u = 3.0 s, and (c) T_u = 5.0 s].

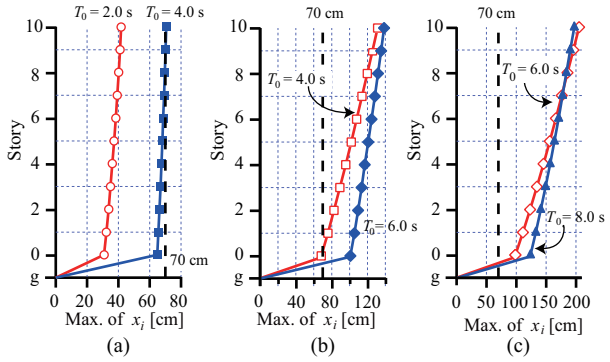

Fig. 11: Maximum displacement of NC for Art Hachinohe wave [(a) T_u = 1.0 s, (b) T_u = 3.0 s, and (c) T_u = 5.0 s].

4.2. Responses for no control

Figs. 10 and 11 show that the maximum displacements of the NC, which does not use any ASC devices, for the Art Kobe and Art Hachinohe waves, respectively. In these figures, 0 on the vertical axes indicates the PBI story, and g means the ground.

The allowable displacement was assumed to be 70 cm in this study, which is the maximal clearance of a building, [24].

These results show that the longer the period of the base isolation is, the larger the displacement is at the PBI story.

As shown in Table 2, the maximum displacement for T_u = 5.0 s for both the Art Hachinohe and Art Kobe waves is larger than 70 cm. Therefore, the PBI alone is not enough to suppress the vibration and an ASC device is necessary.

The responses under the El-Centro and Tokachi waves showed the same trend, and the results are summarized in Appendix C.

4.3. Vibration control of conventional LQR

An ASC device was installed to improve the control performance. An ASC system was designed using the conventional LQR method, that is, minimizing the performance index (6).

This study used three kinds of weights for the performance index (6). The resulting controllers are named LQR 1 [11], LQR 2 [25], and LQR 3 [12]. Q_c for the relative displacement and the relative velocity, and R_c for the control input were set

Table 2: Maximum displacement of NC at the PBI story for Art Hachinohe and Art Kobe waves.

T_u [s]	T_0 [s]	$x_{0\max}$ [cm] (Art Hachinohe)	$x_{0\max}$ [cm] (Art Kobe)
1.0	2.0	30.9	32.3
	4.0	64.8	63.0
3.0	4.0	68.4	57.3
	6.0	100.8	93.9
5.0	6.0	98.4	116.6
	8.0	123.9	148.9

to be

$$\text{LQR 1}: \quad Q_c = \begin{bmatrix} Q_{c1} & \\ & Q_{c2} \end{bmatrix}, \quad R_c = 10^{-\rho}, \tag{16}$$

$$\text{LQR 2}: \quad Q_c = 10^{\rho} \begin{bmatrix} K & \\ & M \end{bmatrix}, \quad R_c = 1, \tag{17}$$

and

$$\text{LQR 3}: \quad Q_c = I_{22}, \quad R_c = 10^{-\rho}. \tag{18}$$

These parameters were selected such that the maximum displacement of the base isolation was almost 50 cm, which is smaller than the allowable range 70 cm, when the Art Hachinohe wave (Fig.7) was input. They are as follows:

- For the model of T_u = 5.0 s and T_0 = 8.0 s:

  LQR 1 :
  $$\begin{cases} \rho = 8.0, \\ Q_{c1} = 0.2 \times \mathrm{diag}\left\{1, 1, 1, 1, 1, 1, 1, 1, 10^3, 1, 10^3\right\}, \\ Q_{c2} = 0.2 \times \mathrm{diag}\left\{1, 1, 1, 1, 1, 1, 1, 1, 10^4, 1, 1\right\}. \end{cases}$$

  $$\text{LQR 2}: \quad \rho = 4.6,$$

  and

  $$\text{LQR 3}: \quad \rho = 9.3.$$

- For the model of T_u = 5.0 s and T_0 = 6.0 s:

  LQR 1 :
  $$\begin{cases} \rho = 8.0, \\ Q_{c1} = 0.2 \times \mathrm{diag}\left\{1, 1, 1, 1, 1, 1, 1, 1, 1, 10^3, 10^3\right\}, \\ Q_{c2} = 0.2 \times \mathrm{diag}\left\{1, 1, 1, 1, 1, 1, 1, 1, 1, 10^3, 10^3\right\}. \end{cases}$$

  $$\text{LQR 2}: \quad \rho = 5.0,$$

  and

  $$\text{LQR 3}: \quad \rho = 9.6.$$

The story-shear coefficient of the i-th story is defined to be

$$q_i = \frac{|V_i(t)|}{\sum_{j=i}^{n} m_j g}, \quad V_i = \sum_{j=i}^{10} f_j. \tag{19}$$

That is, it is a quotient of the story shear V_i at the i-th story and the total weight above the story. V_i is defined as the sum of all

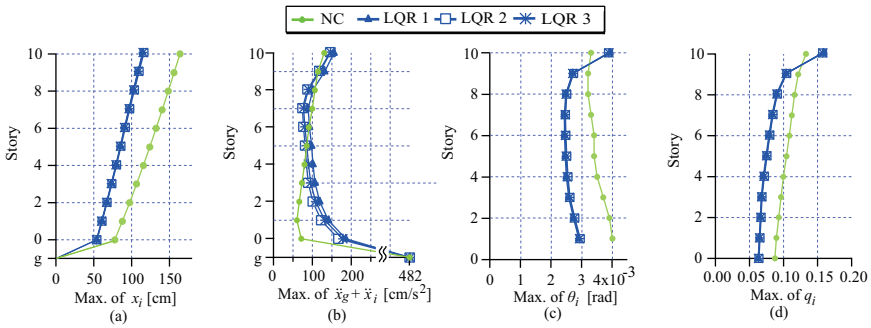

Fig. 12: Comparison of time responses between NC and conventional LQR for T_0 = 6.0 s for Art Kobe wave.

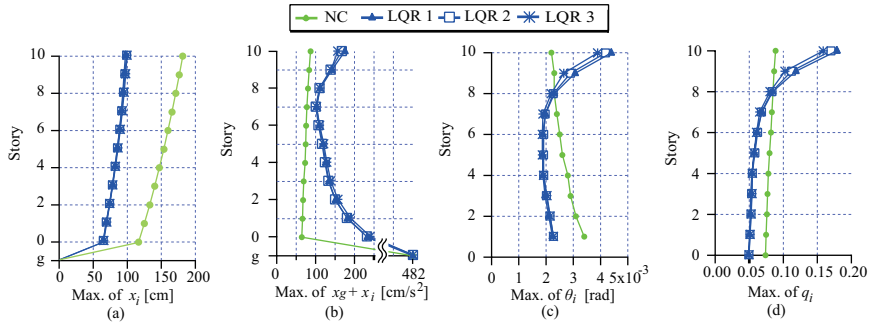

Fig. 13: Comparison of time responses between NC and conventional LQR for T_0 = 8.0 s for Art Kobe wave.

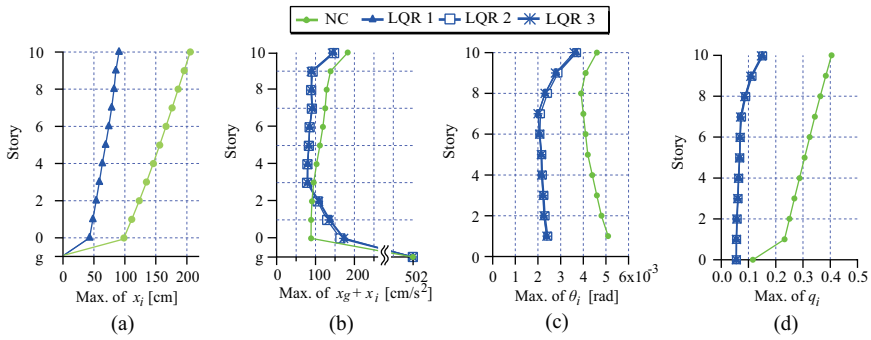

Fig. 14: Comparison of time responses between NC and conventional LQR for T_0 = 6.0 s for Art Hachinohe wave.

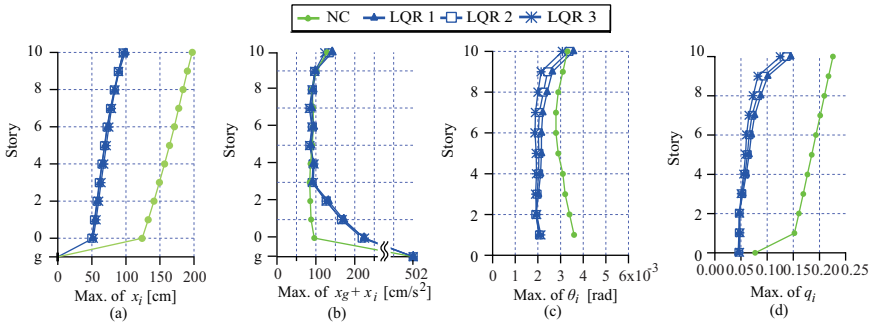

Fig. 15: Comparison of time responses between NC and conventional LQR for T_0 = 8.0 s for Art Hachinohe wave.

lateral force above the story, and f_i is the lateral force in the fundamental mode acting on the j-th story.

Figs. 12 and 13 show the responses for the Art Kobe wave, and Figs. 14 and 15 show those for the Art Hachinohe wave for different T_0.

Figs. 12 (a) and 13 (a) show that the maximum displacement of the PBI story of LQRs 1-3 for the Art Kobe wave are 54.1 cm, 53.6 cm, and 54.1 cm for T_0 = 6.0 s, respectively; and 63.3

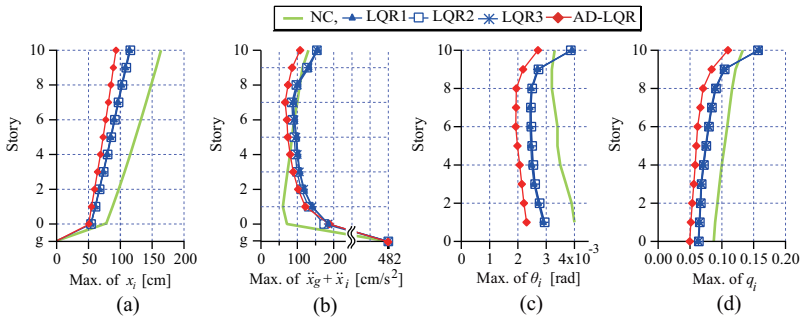

Fig. 16: Comparison of time responses between LQRs 1-3 and AD-LQR for T_0 = 6.0 s for Art Kobe wave.

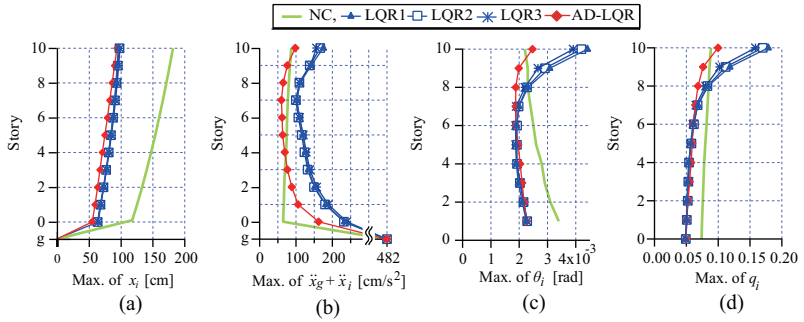

Fig. 17: Comparison of time responses between LQRs 1-3 and AD-LQR for T_0 = 8.0 s for Art Kobe wave.

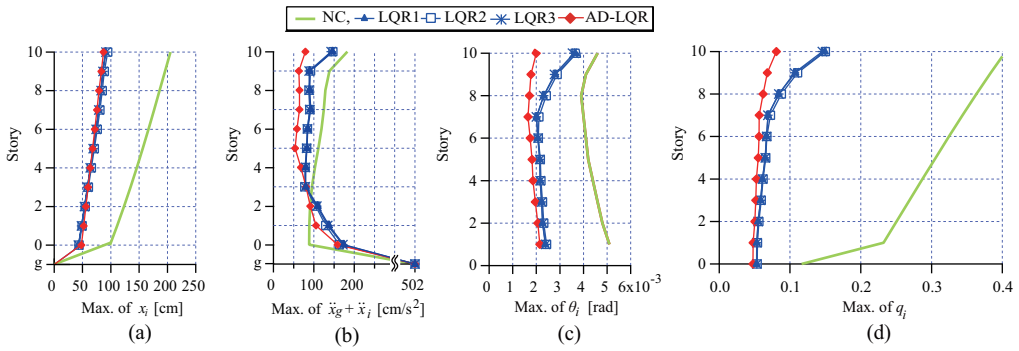

Fig. 18: Comparison of time responses between LQRs 1-3 and AD-LQR for T_0 = 6.0 s for Art Hachinohe wave.

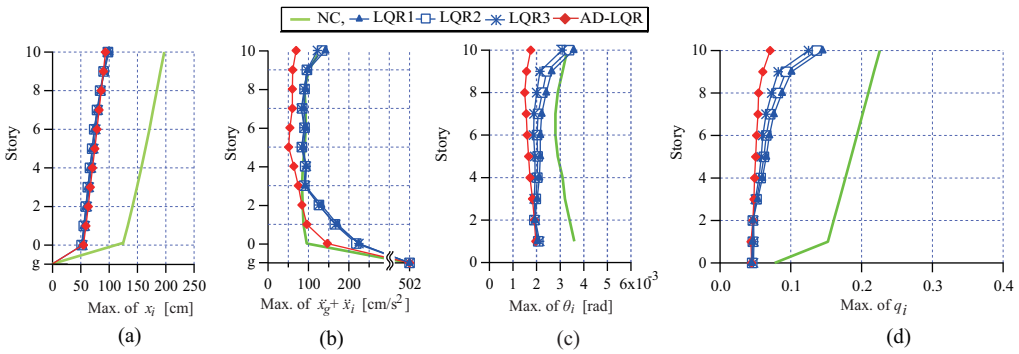

Fig. 19: Comparison of time responses between LQRs 1-3 and AD-LQR for T_0 = 8.0 s for Art Hachinohe wave.

cm, 64.0 cm, and 63.0 cm for T_0 = 8.0 s, respectively. The maximum displacement of the PBI story are in the allowable range. The displacement of the tenth story for the conventional LQR is suppressed to about 50% of that for the NC for T_0 = 8.0 s. This shows that LQRs 1-3 have good vibration-control performance.

As for the Art Hachinohe wave (Figs. 14 and 15), the maximum displacement of LQRs 1-3 of the PBI story are 43.0 cm, 42.8 cm, and 43.9 cm for $T_0 = 6.0$ s, respectively; and 52.0 cm, 53.5 cm, and 51.2 cm for $T_0 = 8.0$ s, respectively, which are also in the allowable range. The displacement of the higher story tended to become larger than that of the lower story. The maximum of the inter-story drift angles and the story-shear coefficients for the conventional LQR for $T_0 = 6.0$ s are almost all suppressed to less than 50% of those for the NC. Furthermore, for LQRs 1, 2, and 3 for $T_0 = 8.0$ s, the maximums of the displacements and the story-shear coefficients of the top story are also suppressed to as low as approximately 40% of those for the NC.

For each earthquake, the control performances of LQRs 1-3 for displacement are satisfactory. However, for each earthquake, the inter-story drift angles of the higher stories for LQRs 1-3 are larger than those for the lower stories. Although suppressing inter-story angles and absolute acceleration are important to protect the building and people, the performance indices of LQRs 1, 2 and 3 do not take those items into account. In contrast, the AD-LQR method includes those in the performance index. A comparison of LQRs 1-3 and the AD-LQR is shown in the next section.

4.4. Vibration control of AD-LQR

The weights Q_g for the absolute acceleration, Q_d for the inter-story drift and the inter-story velocity, and R_u for the control input in (8) were set to be

$$Q_g = 10^{\alpha} I_{11},\ Q_d = 10^{\beta} \times \begin{bmatrix} Q_{d1} & \\ & Q_{d2} \end{bmatrix},\ R_u = I_{11}. \qquad (20)$$

The parameters were selected as follows

- For the model with $T_u = 5.0$ s and $T_0 = 8.0$ s:

$$\begin{cases} \alpha = 12,\ \beta = 12.5, \\ Q_{d1} = \mathrm{diag}\left\{1, 1, 1, 1, 1, 1, 1, 1, 10^{1.5}, 10^{1.5}, 10^{1.4}\right\}, \\ Q_{d2} = \mathrm{diag}\left\{1, 1, 1, 1, 1, 1, 1, 1, 10^{1.5}, 10^{1.5}, 10^{1.4}\right\}. \end{cases}$$

- For the model with $T_u = 5.0$ s and $T_0 = 6.0$ s:

$$\begin{cases} \alpha = 12.7,\ \beta = 14 \\ Q_{d1} = \mathrm{diag}\left\{10^{0.2}, 1, 1, 1, 1, 1, 1, 1, 10^{1.5}, 10^{1.5}, 10^{1.4}\right\}, \\ Q_{d2} = \mathrm{diag}\left\{10^{0.2}, 1, 1, 1, 1, 1, 1, 1, 10^{1.5}, 10^{1.5}, 10^{1.4}\right\}. \end{cases}$$

These AD-LQR controllers were designed such that the maximum displacement of each story is almost the same as that of LQRs 1-3 when the Art Hachinohe wave was input.

Figs. 16(a) and 17(a) show that the maximum displacement of the story of the AD-LQR is 50.5 cm for $T_0 = 6.0$ s, and 57.4 cm $T_0 = 8.0$ s. They are all in the allowable range. As for $T_0 = 8.0$ s, the control results of the inter-story drift angles and the absolute acceleration are smaller for the AD-LQR than for LQRs 1-3. The absolute acceleration for the AD-LQR is about 50% of that for each of LQRs 1-3 [Fig. 18(b)], and the inter-story drift angle of the tenth story for the AD-LQR is also only 50% of that for each of LQRs 1-3 [Fig. 18(c)]. Figs. 18 and 19 show the results for the Art Hachinohe wave. The maximum displacement of the story of the PBI for the AD-LQR is 47.8 cm for $T_0 = 6.0$ s and 54.6 cm for $T_0 = 8.0$ s. They are also all in the allowable range. They show the same trend for the Art Kobe wave for $T_0 = 8.0$ s. The displacement, the absolute acceleration, the inter-story-drift angles, and the story-shear coefficient of LQRs 1-3 are almost the same even though the weights are different. However, the control performance of the AD-LQR for these responses is better than that for each of LQRs 1-3. Thus, the AD-LQR is more appropriate than the LQR that considers only the relative displacement and the relative velocity.

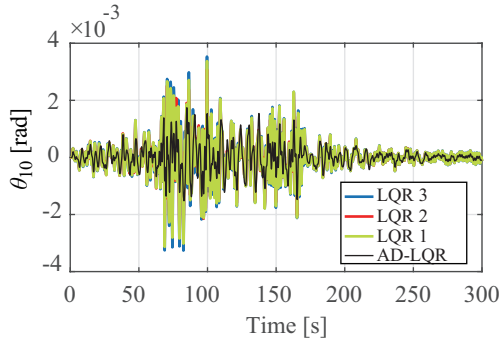

Fig. 20: Time response of inter-story drift angle of tenth story for Art Hachinohe wave ($T_u = 5.0$ s and $T_0 = 8.0$ s).

Table 3: Maximum and minimum inter-story drift angles of the tenth story, θ_{10} [rad] ($\times 10^{-3}$).

	Max.	Min.
AD-LQR	1.74	−1.52
LQR 1	3.53	−3.26
LQR 2	3.08	−2.97
LQR 3	3.37	−3.13

Figs. 16-19 show that, compared to LQRs 1-3, the control effects for AD-LQR are markedly improved for higher stories.

The time responses of the inter-story drift angle of the top story (Fig. 20) shows that the response for the AD-LQR is smaller than that for LQRs 1-3. Table 3 shows the detailed data of Fig. 20. The control performance of the inter-story drift angles for the AD-LQR is better than that for LQRs 1-3, especially for the tenth story. For each earthquake, the maximum displacement is approximately the same for the AD-LQR and LQRs 1-3 for $T_0 = 6.0$ s. However, the absolute acceleration and the inter-story drift angles for $T_0 = 8.0$ s for the AD-LQR are better than those for LQRs 1-3, especially those for the tenth story. One reason for this observation is that, compared to LQRs 1-3, the AD-LQR increased the damping ratios of the lower modes considerably.

Fig. 21 shows the control input of the AD-LQR and LQRs 1-3 for $T_0 = 8.0$ s for the Art Hachinohe wave. While the control inputs are almost the same (the control input of the AD-LQR is only 1.2 times better than that of LQRs 1-3) and the shapes are also same, the maximum absolute acceleration, the inter-story drift angles, and the story-shear coefficients for the AD-LQR

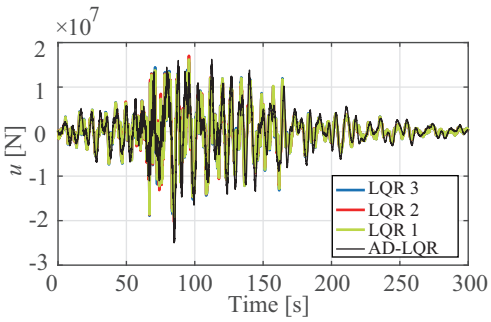

Fig. 21: Control inputs for Art Hachinohe wave (T_u = 5.0 s and T_0 = 8.0 s).

Table 4: Maximum and minimum control inputs, u [N] ($\times 10^7$).

	Max.	Min.
AD-LQR	1.62	−2.50
LQR 1	1.56	−1.89
LQR 2	1.70	−2.03
LQR 3	1.62	−1.92

are smaller than those for LQRs 1-3. Table 4 shows the detailed data of Fig. 21.

5. Discussion of control performance

In this section, the control results given in Section 4 are examined from the viewpoint of the pole-zero plot and the damping ratio of the control system.

5.1. Observation from system zeros

Let a transfer function $G(s)$ be

$$G(s) = \frac{N(s)}{D(s)} = K_g \frac{\prod_{j=1}^{n_z}(s + z_j)}{\prod_{i=1}^{n_p}(s + p_i)}, \tag{21}$$

where s is the operator of the Laplace transform; $N(s)$ is the numerator polynomial of $G(s)$ in s with order of n_z, and $D(s)$ is the denominator polynomial of $G(s)$ in s with order of n_p. Without loss of generality, $G(s)$ is strictly proper, that is, n_p is bigger than n_z.

The roots of

$$D(s) = 0 \tag{22}$$

and

$$N(s) = 0 \tag{23}$$

are called the poles and zeros of $G(s)$, respectively. Poles determine the stability of the system. If all poles have negative real parts, the system is stable. On the other hand, zeros affect the characteristics of the response of the system. If all zeros have negative real parts, the system is called a minimum-phase system, and is easy to control [28]. However, if a system has unstable zeros, that is, those zeros have positive real parts, it

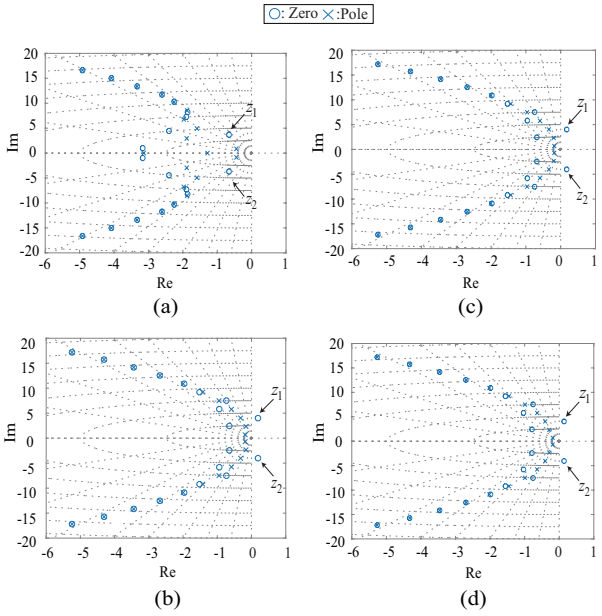

Fig. 22: Pole-zero plot of $G_{10g}(s)$ [(a) AD-LQR, (b) LQR 1, (c) LQR 2, and (d) LQR 3] (T_u = 5.0 s and T_0 = 8.0 s).

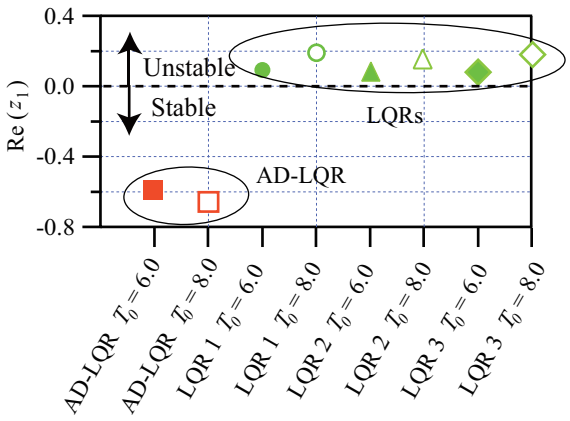

Fig. 23: Zero plot of LQRs 1-3 and AD-LQR.

is called a non-minimum phase system. The behavior of such a system is complicated and it is difficult to control (See Appendix A).

Fig. 22 shows the pole-zero plot of the transfer function from the earthquake input to the displacement of the tenth story, $G_{10g}(s)$, for T_u = 5.0 s and T_0 = 8.0 s, in which a pole and a zero are marked by a circle and a cross, respectively. Let the conjugate zeros that are closest to the imaginary axis be z_1 and z_2. It is clear from Fig. 22 that, while each of LQRs 1-3 have two conjugate unstable zeros, the AD-LQR does not. This also shows why the AD-LQR has better control performance than LQRs 1-3.

Fig. 23 shows the real part of $G_{10g}(s)$ for the control systems designed by LQRs 1-3 and the AD-LQR. Clearly, while z_1 and z_2 designed by LQRs 1-3 are all unstable for different T_0, those zeros designed by the AD-LQR are all stable, and have a relatively big negative real part.

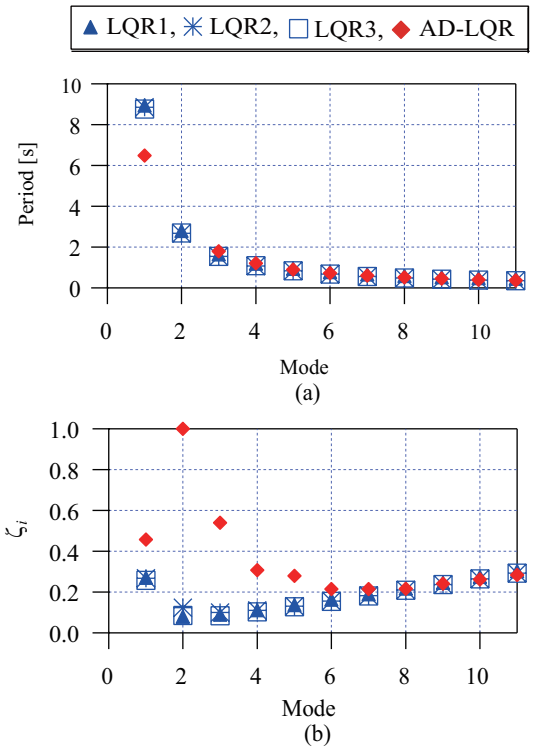

Fig. 24: Comparison between LQRs 1-3 and AD-LQR (T_u = 5.0 s and T_0 = 8.0 s) [(a) damping ratio and (b) natural period].

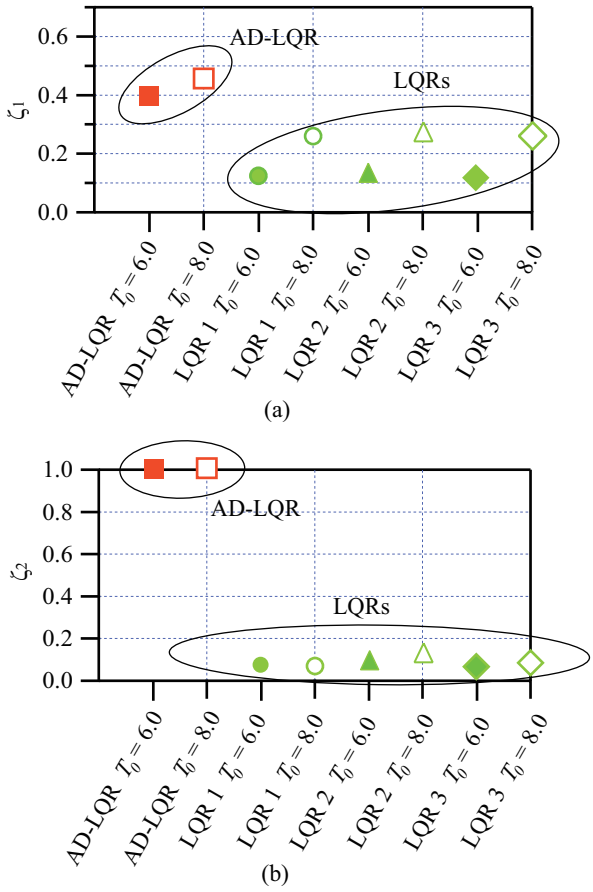

Fig. 25: Damping ratio of AD-LQR and LQRs 1-3 for (a): the first mode and (b): the second mode.

Figs. 22 and 23 show that the performance index that only considers the relative displacement and the relative velocity may introduce unstable zeros. The control performance of the AD-LQR for the inter-story-drift angle and the story-shear coefficient at the tenth story is better than that for LQRs 1-3. One of the reasons is that the transfer functions of LQRs 1-3 have unstable zeros.

5.2. Analysis of damping ratio and natural period

Fig. 24 shows the natural period and the damping ratio of the i-th mode, ζ_i, for LQRs 1-3 and the AD-LQR for T_0 = 8.0 s. They are given by

$$\zeta_i = \frac{-\mathrm{Re}(p_i)}{\sqrt{\mathrm{Re}(p_i)^2 + \mathrm{Im}(p_i)^2}}, \; T_i = \frac{2\pi}{\sqrt{\mathrm{Re}(p_i)^2 + \mathrm{Im}(p_i)^2}}, \quad (24)$$

where, $\mathrm{Re}(p_i)$ and $\mathrm{Im}(p_i)$ are the real and the imaginary parts of the i-th pole, respectively. It is clear from Fig. 24 that the natural periods are almost the same for both the LQRs 1-3 and the AD-LQR except for the first mode. However, the damping ratios of the AD-LQR for the first to the third modes are bigger than those for LQRs 1-3. In particular, the damping ratio of the first mode for the AD-LQR is 1.7 times, the second mode is 14.5 times, and the third mode is 7 times larger than those for LQRs 1-3. The AD-LQR has good damping ratio especially for the second mode.

As a result, Fig. 20 shows that the response of the AD-LQR is smaller than that of LQRs 1-3. Fig. 25(a) shows the damping ratios for the first modes of LQRs 1-3 and the AD-LQR for T_0 = 6.0 s and 8.0 s with T_u = 5.0 s. It is clear from the figure that the damping ratios for the AD-LQR are larger than those for LQRs 1-3. The damping ratio of the first mode for the AD-LQR for T_0 = 6.0 s is also more than two times larger than that for LQRs 1-3 for T_0 = 6.0 s. Fig. 25(b) shows the damping ratios for the second mode of the LQR and the AD-LQR for T_0 = 6.0 s and 8.0 s with T_u = 5.0 s. The damping ratio for the second mode of each AD-LQR is almost 1.0. Thus, the control performance of the AD-LQR for the first and second modes is better than those for the conventional LQR. As the first and second modes mainly influence the PBI of a building, and the second mode mainly influences the absolute acceleration [26], the increase in the damping ratio by the AD-LQR results in good control performance of the absolute acceleration, the inter-story drifts, and the story-shear coefficients (Figs. 16-19). LQRs 1-3 had unstable zeros, which caused undesirable vibrations in the time responses. However, the AD-LQR did not have any unstable zeros. Moreover, the damping ratio for each mode of the AD-LQR was larger than that of LQRs 1-3. As a result, Figs. 16-19 show that the responses of the AD-LQR at the upper story are smaller than those of LQRs 1-3 for all the earthquake waves.

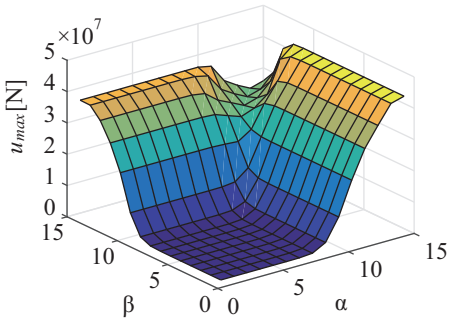

Fig. 26: Relationship between α, β, and maximum control input for Art Hachinohe wave (T_u = 5.0 s and T_0 = 8.0 s).

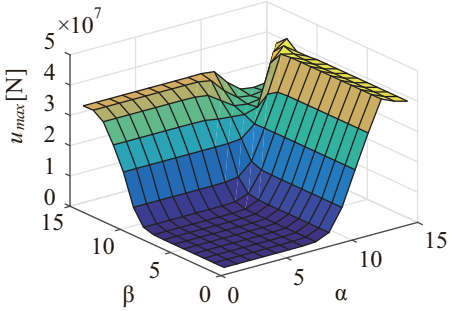

Fig. 27: Relationship between α, β, and maximum control input for Art Kobe wave (T_u = 5.0 s and T_0 = 8.0 s).

6. Selection of weights for the AD-LQR

The performance index of the AD-LQR is formed by the weighted sum of the absolute acceleration, the inter-story drifts, and the inter-story velocity. The weights also have a considerable effect on control performance. This point is examined in this section.

The H_∞ norm of the transfer function from the earthquake input to a variable of the building, $G(s)$, is

$$\|G\|_\infty = \max_{0\le\omega\le+\infty} \sigma_{\max}(G(j\omega)), \tag{25}$$

where $\sigma_{\max}(G)$ is the maximum singular value of G [29]. This study used $1/\|G\|_\infty$ as a criterion for the selection of weights. A large $1/\|G\|_\infty$ means a good control performance. In this paper, three transfer functions are considered: the transfer function from the earthquake input to the absolute acceleration of the top story, G_a; to the inter-story drift angle of the top story, G_i; and to the displacement of the PBI story, G_d.

The factor α in the weight Q_g in (20) is related to the absolute acceleration; and β in Q_d, to the inter-story drift angles. We try to examine the relationships between the factors α and β, and the maximum control input;, and the relationships between the factors *alpha* and *beta*, and the function $1/\|G_a\|_\infty$, to $1/\|G_i\|_\infty$, and to $1/\|G_d\|_\infty$.

Figs. 26 and 27 show the relationship between the weight factors, α and β, and the maximum control input. It is clear from the figure that the maximum control input becomes large as α and β become large.

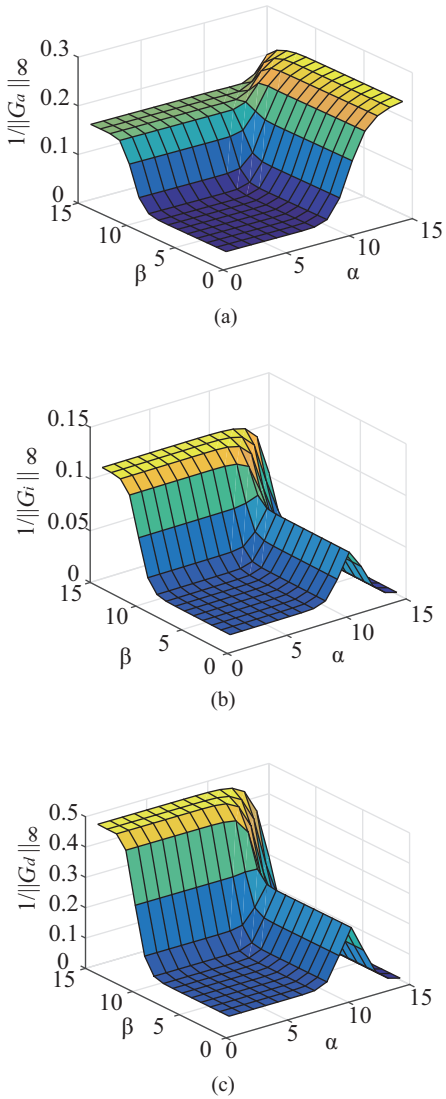

Fig. 28: Relationship between α, β, and control performance [(a) Absolute acceleration, (b) Inter-story drift angle, and (c) Displacement of PBI (T_u = 5.0 s and T_0 = 8.0 s)].

Fig. 28 (a)-(c) show the relationship between those factors and $1/\|G_a\|_\infty$, $1/\|G_i\|_\infty$, and $1/\|G_d\|_\infty$ for T_0 = 8.0 s for the Art Hachinohe wave. These figures show that, when α and β are around 13, $1/\|G_a\|_\infty$, $1/\|G_i\|_\infty$, and $1/\|G_d\|_\infty$ are all very large. However, this is impossible for passive structural control because there is a trade-off between the control performance of the absolute acceleration and the displacement. It is also worth mentioning that a further increase in α and β may not necessarily result in better control performance.

7. Conclusion

This paper considered the issue of carrying out structural control for a high-rise building using a combination of the PBI and the ASC. Unlike a conventional LQR controller, which was represented by LQRs 1-3 in this study, the LQR controller was designed by choosing the performance indices that contain the

absolute acceleration, inter-story drifts and velocity of the stories. The effects of this method were examined through analyses of the time-domain response, damping ratios of modes, and locations of system zeros. Furthermore, the selection of the weights was examined by using the H_∞-norm-based criteria. This study clarified the following points:

- This study presented a new performance index for LQRs, which is called the AD-LQR. While a performance index for a conventional LQR considers the relative displacement and the relative velocity of a building, the AD-LQR considers the absolute acceleration, the inter-story velocity, and the inter-story drifts. This allows us to design an ASC system that suppresses not only relative displacement but also the absolute acceleration. This reduces the impact on both a building and the people inside it.
- The comparison between the damping ratios of LQRs 1-3 and the AD-LQR showed that the damping ratios of the first to the third modes for the AD-LQR were bigger than those of LQRs 1-3. The AD-LQR resulted in a small absolute acceleration and inter-story drifts compared to LQRs 1-3.
- The comparison of the zeros of the transfer function from the earthquake input into the displacement of the tenth story showed that, while the transfer functions for LQRs 1-3 had unstable zeros, the transfer function for the AD-LQR did not. Thus, the AD-LQR was easier to control compared to LQRs 1-3.
- When the weights of the absolute acceleration, and the inter-story drifts and velocity increased in a certain range, the maximum control input increased. A suitable selection of these weights provided satisfactory control performance for the absolute acceleration and the inter-story drift angles simultaneously.

Appendix A. Nonminimum phase system [23]

For example, consider the following system

$$G(s) = \frac{\epsilon s^2 - \eta s + 1}{(s+5)(s^2+2s+1)}, \tag{A.1}$$

where ϵ and η are real constants. If $\epsilon = 0$, the system has one zero given by

$$z = \frac{1}{\eta}.$$

The step responses of the system for η being ± 1 and ± 2 (Fig. A.29) show that an unstable zero ($\eta = 1, 2$) has a major effect on the transient response and causes an undershoot. On the other hand, the system has two zeros if $\epsilon \neq 0$. They are given by

$$z_{1,2} = \frac{\eta \pm \sqrt{\eta^2 - 4\epsilon}}{2\epsilon}. \tag{A.2}$$

The step response of the system for $\epsilon = 0.5$ and $\eta = \pm 1$ or ± 2 (Fig. A.30) shows that the outputs for unstable zeros ($\eta = 1, 2$) are positive first, then negative, and finally positive. Thus, an increase in the number of unstable zeros makes the transient response complicated.

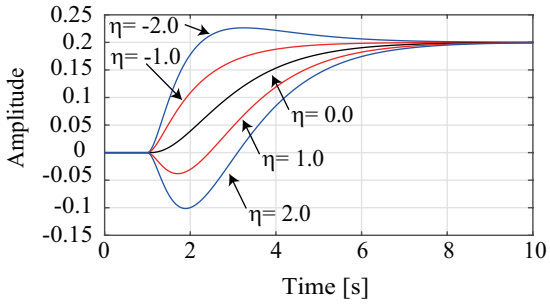

Fig. A.29: Step responses for system (A.1) with one zero.

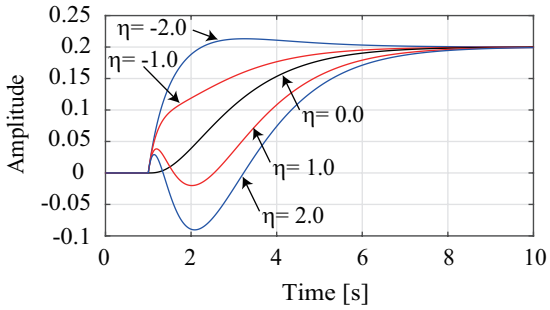

Fig. A.30: Step responses for system (A.1) with two zeros.

Appendix B. Responses for the Art Kobe and Art Hachinohe waves

The detailed data of Figs. 16-19 are shown in Tables B.5-B.8.

Appendix C. Responses for the El-Centro and Tokachi waves

The time responses for the El-Centro and the Tokachi waves are shown in Figs. C.31 - C.34. The detailed data of these figures are shown in Tables C.9-C.12. The relationships between the weight factors, α and β, and the maximum control input for these waves are shown in Figs. C.35 and C.36. These tables show that the displacements are almost all the same for the AD-LQR and LQRs 1-3. However, the absolute acceleration, the inter-story drift angles, and the story-shear coefficients of the AD-LQR are smaller than those of LQRs 1-3, especially those of the upper stories. These results have the same trend as the results for the Art Hachinohe and Kobe waves.

References

[1] J.M. Kelly, Earthquake-Resistant Design with Rubber. Springer, 1997.

[2] D. Forcellini, J.M. Kelly, Analysis of the large deformation stability of elastomeric bearings, J Eng Mech 140 (6) (2014) 1-10.

[3] The Japan Society of Seismic Isolation, Recent Trends in Seismic Isolation Buildings. ¡http://www.jssi.or.jp/menshin/doc/keizoku2.pdf¿ [in Japanese].

Table B.5: Maximums of responses for Art Kobe wave (T_0 = 6.0 s).

	Story	0	1	2	3	4	5	6	7	8	9	10
x [cm]	NC	116.6	125.0	132.9	140.2	147.1	153.6	159.7	165.6	171.1	176.4	181.4
	AD-LQR	50.5	54.7	59.6	64.3	68.7	73.0	77.1	81.3	85.3	89.1	93.2
	LQR 1	54.1	60.7	67.0	73.3	79.3	85.0	90.4	96.1	101.9	107.9	114.2
	LQR 2	53.6	60.4	66.8	73.1	79.2	85.0	90.6	96.4	102.3	108.4	114.8
	LQR 3	54.1	61.0	67.5	73.9	80.0	85.8	91.5	97.3	103.3	109.5	115.8
$\ddot{x}+\ddot{x}_g$ [cm/s^2]	NC	71.4	60.3	66.4	72.9	79.7	85.4	91.2	99.8	106.3	114.3	130.4
	AD-LQR	188.2	121.9	102.3	88.6	80.2	73.6	71.2	66.4	74.6	85.6	107.5
	LQR 1	185.5	141.4	118.7	106.8	101.5	97.8	92.7	89.2	101.3	131.6	155.4
	LQR 2	184.4	140.1	117.2	105.2	99.6	95.8	90.8	87.5	99.7	129.2	154.2
	LQR 3	173.7	131.3	110.2	99.3	94.5	91.6	87.4	84.8	97.4	126.7	153.7
θ [rad] ($\times 10^{-3}$)	NC	—	4.04	3.85	3.67	3.54	3.44	3.36	3.27	3.20	3.16	3.27
	AD-LQR	—	2.31	2.21	2.14	2.06	1.99	1.92	1.93	1.94	2.18	2.71
	LQR 1	—	2.90	2.73	2.57	2.49	2.46	2.43	2.42	2.47	2.69	3.91
	LQR 2	—	2.92	2.75	2.59	2.52	2.49	2.46	2.46	2.48	2.70	3.88
	LQR 3	—	2.95	2.77	2.61	2.55	2.50	2.47	2.46	2.50	2.73	3.87
q ($\times 10^{-2}$)	NC	8.73	8.96	9.31	9.64	9.99	10.4	10.8	11.2	11.6	12.1	13.3
	AD-LQR	4.97	5.13	5.37	5.61	5.83	6.00	6.20	6.63	7.06	8.39	11.0
	LQR 1	6.28	6.44	6.60	6.73	7.03	7.42	7.84	8.31	8.96	10.3	15.9
	LQR 2	6.33	6.49	6.66	6.80	7.11	7.51	7.94	8.41	9.02	10.3	15.7
	LQR 3	6.39	6.54	6.70	6.84	7.18	7.57	7.98	8.43	9.09	10.5	15.7

Table B.6: Maximums of responses for Art Kobe wave (T_0 = 8.0 s).

	Story	0	1	2	3	4	5	6	7	8	9	10
x [cm]	NC	77.7	87.8	97.4	106.6	115.5	124.0	132.4	140.5	148.5	156.2	163.9
	AD-LQR	57.4	61.7	65.7	70.1	74.6	78.8	82.9	87.0	90.8	94.5	98.1
	LQR 1	63.3	67.8	72.5	76.7	80.5	83.9	87.0	89.8	92.0	93.7	95.8
	LQR 2	64.0	68.3	72.9	77.3	81.2	84.8	88.2	91.4	94.0	96.2	98.1
	LQR 3	63.0	67.5	72.3	76.6	80.5	84.0	87.3	90.3	92.7	94.8	97.4
$\ddot{x}+\ddot{x}_g$ [cm/s^2]	NC	64.5	66.3	67.7	69.5	72.8	74.4	75.7	77.4	80.4	83.2	86.9
	AD-LQR	162.2	105.9	88.3	76.3	69.1	63.4	61.9	59.9	64.7	75.9	97.9
	LQR 1	233.3	181.6	151.3	134.3	125.8	118.7	109.5	102.1	111.6	141.5	175.1
	LQR 2	239.5	188.5	156.7	138.2	128.3	119.9	109.5	101.6	110.5	139.4	156.4
	LQR 3	231.7	179.6	149.2	132.0	123.1	115.8	106.7	99.5	109.1	137.9	166.7
θ [rad] ($\times 10^{-3}$)	NC	—	3.36	3.13	2.93	2.76	2.64	2.52	2.42	2.33	2.25	2.20
	AD-LQR	—	2.26	2.17	2.10	2.04	1.96	1.88	1.88	1.88	1.99	2.47
	LQR 1	—	2.25	2.11	1.97	1.90	1.89	1.90	1.99	2.31	3.08	4.41
	LQR 2	—	2.28	2.16	2.05	1.92	1.87	1.88	1.90	2.20	2.66	3.91
	LQR 3	—	2.28	2.15	2.03	1.92	1.92	1.92	1.98	2.28	2.91	4.20
q ($\times 10^{-2}$)	NC	7.38	7.47	7.59	7.70	7.81	7.99	8.17	8.33	8.49	8.64	8.86
	AD-LQR	4.95	5.01	5.26	5.52	5.75	5.94	6.07	6.43	6.83	7.64	9.99
	LQR 1	4.86	5.00	5.11	5.18	5.36	5.72	6.12	6.83	8.43	11.8	17.9
	LQR 2	4.93	5.09	5.24	5.37	5.42	5.67	6.05	6.49	8.03	10.2	15.8
	LQR 3	4.92	5.08	5.22	5.32	5.43	5.80	6.20	6.78	8.30	11.2	17.0

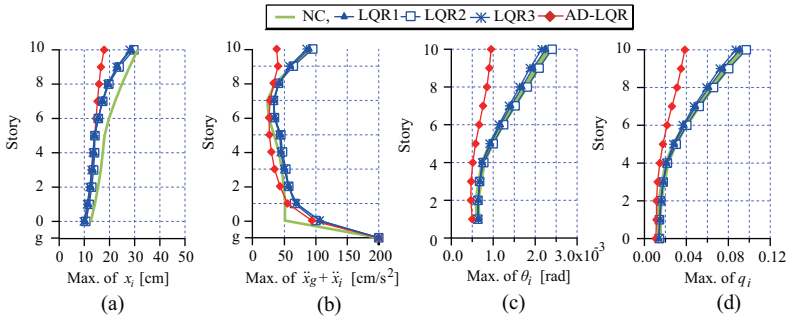

Fig. C.31: Comparison of time responses between LQRs 1-3 and AD-LQR for T_0 = 6.0 s for Tokachi wave.

[4] D. Foti, A. Catalan Goni, S. Vacca, On the dynamic response of rolling base isolation systems, Struct Control and Health Monitor 20 (4) (2013) 639-648.

[5] N. Menga, D. Foti, G. Carbone, Viscoelastic frictional properties of rubber-layer roller bearings (RLRB) seismic isolators, Meccanica 52 (11-12) (2017) 2807-2817.

[6] D. Foti, M. Diaferio, R. Nobile, Dynamic Behavior of New Aluminum-Steel Energy Dissipating Devices, Struct Control and Health Monitor 20 (7) (2013) 1106-1119.

[7] D. Foti, M. Diaferio, R. Nobile, Optimal design of a new seismic passive protection device made in aluminium and steel, Int J Struct Eng Mech 35 (1) (2010) 119-122.

Table B.7: Maximums of responses for Art Hachinohe wave (T_0 = 6.0 s).

	Story	0	1	2	3	4	5	6	7	8	9	10
x [cm]	NC	98.4	111.2	123.3	134.8	145.8	156.3	166.5	176.4	186.0	195.6	205.3
	AD-LQR	47.8	52.1	56.0	59.7	63.7	67.7	71.6	75.4	79.2	83.1	87.0
	LQR 1	43.0	48.3	53.6	58.7	63.6	68.9	74.0	78.6	82.4	85.5	90.4
	LQR 2	42.8	48.1	53.5	58.7	63.7	69.0	74.2	78.9	82.9	86.4	91.6
	LQR 3	43.9	49.5	55.0	60.2	65.5	70.8	76.0	80.8	84.8	88.5	94.4
$\ddot{x} + \ddot{x}_g$ [cm/s^2]	NC	88.2	88.6	90.6	95.3	102.8	111.2	119.0	124.6	128.4	138.7	182.8
	AD-LQR	158.7	105.2	91.1	80.6	68.0	53.6	58.4	64.6	64.5	62.7	79.0
	LQR 1	174.0	137.4	109.6	79.9	79.9	83.1	84.9	92.3	89.9	90.1	146.2
	LQR 2	171.7	134.4	107.2	78.7	78.9	82.3	84.2	89.9	88.4	88.3	142.8
	LQR 3	163.3	129.4	104.6	77.6	78.5	82.2	84.2	90.0	87.8	91.7	147.0
θ [rad] ($\times 10^{-3}$)	NC	—	5.08	4.82	4.58	4.38	4.19	4.05	3.95	3.93	4.11	4.58
	AD-LQR	—	2.15	2.07	1.96	1.86	1.82	1.74	1.65	1.70	1.77	2.00
	LQR 1	—	2.38	2.26	2.23	2.16	2.14	2.06	2.01	2.32	2.81	3.69
	LQR 2	—	2.39	2.27	2.23	2.16	2.15	2.08	2.00	2.32	2.77	3.60
	LQR 3	—	2.43	2.32	2.26	2.19	2.17	2.09	2.11	2.42	2.89	3.71
q ($\times 10^{-2}$)	NC	11.1	11.3	11.7	12.1	12.4	12.8	13.1	13.6	14.3	15.8	18.7
	AD-LQR	4.75	4.79	5.02	5.15	5.25	5.50	5.62	5.65	6.19	6.80	8.06
	LQR 1	5.27	5.29	5.48	5.84	6.10	6.48	6.65	6.90	8.41	10.8	14.9
	LQR 2	5.30	5.32	5.50	5.84	6.11	6.51	6.71	6.88	8.42	10.6	14.6
	LQR 3	5.37	5.41	5.61	5.94	6.19	6.56	6.73	7.23	8.78	11.1	15.0

Table B.8: Maximums of responses for Art Hachinohe wave (T_0 = 8.0 s).

	Story	0	1	2	3	4	5	6	7	8	9	10
x [cm]	NC	123.9	132.8	141.2	149.2	156.8	164.1	171.0	177.6	184.0	190.4	197.3
	AD-LQR	54.7	59.0	63.0	66.8	70.6	74.6	78.5	82.3	85.9	89.8	93.5
	LQR 1	52.0	55.8	59.4	62.8	66.5	70.3	74.0	79.0	85.0	91.6	99.8
	LQR 2	53.5	57.6	61.3	64.8	68.8	72.7	76.3	80.4	85.4	90.7	97.2
	LQR 3	51.2	55.2	58.8	62.3	66.1	70.0	73.7	78.6	84.2	90.2	97.7
$\ddot{x} + \ddot{x}_g$ [cm/s^2]	NC	95.8	87.4	85.5	84.1	85.9	90.7	93.3	92.8	89.8	101.6	128.7
	AD-LQR	146.8	96.1	83.9	74.7	63.6	51.1	53.9	60.1	60.3	60.9	69.5
	LQR 1	223.7	171.8	132.0	91.5	94.0	86.9	94.2	88.7	93.0	98.8	142.0
	LQR 2	224.5	166.9	125.8	92.6	94.5	83.3	89.2	82.5	89.7	96.5	122.5
	LQR 3	218.5	165.3	126.0	89.5	91.9	83.7	90.3	84.3	90.4	96.1	134.0
θ [rad] ($\times 10^{-3}$)	NC	—	3.59	3.40	3.23	3.06	2.92	2.82	2.82	2.90	3.04	3.23
	AD-LQR	—	1.96	1.91	1.83	1.72	1.66	1.60	1.56	1.50	1.58	1.75
	LQR 1	—	2.04	1.92	2.02	2.12	2.16	2.16	2.22	2.40	2.64	3.58
	LQR 2	—	2.13	1.94	1.90	1.94	1.92	1.87	1.89	2.01	2.14	3.08
	LQR 3	—	2.07	1.90	1.97	2.03	2.04	2.02	2.07	2.24	2.43	3.37
q ($\times 10^{-2}$)	NC	7.84	7.97	8.25	8.48	8.66	8.84	9.13	9.71	10.6	11.7	13.1
	AD-LQR	4.45	4.38	4.63	4.79	4.86	5.03	5.17	5.35	5.44	6.05	7.07
	LQR 1	4.45	4.57	4.65	5.31	5.99	6.54	6.96	7.61	8.76	10.1	14.5
	LQR 2	4.72	4.78	4.73	4.98	5.48	5.83	6.05	6.50	7.29	8.22	12.5
	LQR 3	4.54	4.64	4.63	5.16	5.74	6.19	6.52	7.09	8.17	9.32	13.7

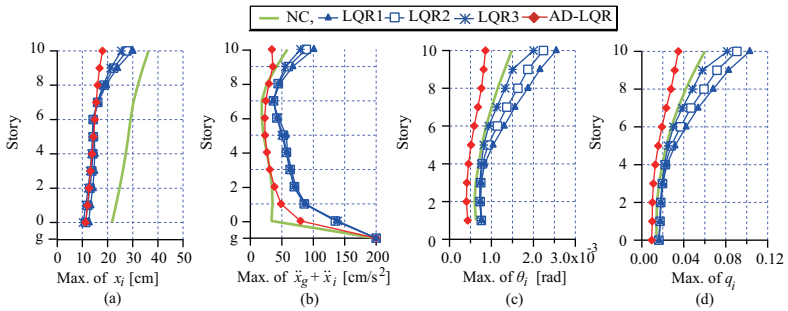

Fig. C.32: Comparison of time responses between LQRs 1-3 and AD-LQR for T_0 = 8.0 s for Tokachi wave.

[8] D. Foti, L.M. Bozzo, F. Lopez-Almansa, Numerical efficiency assessment of energy dissipators for seismic protection of buildings, Earthquake Eng Struct Dyn 27 (1998) 543-556.

[9] S. Korkmaz, A review of active structural control: challenges for engineering informatics, Comput Struct 89 (2011) 2113-2132.

[10] F. Casciati, J. Rodellar, U. Yildirim, Active and semi-active control of structures– theory and applications: a review of recent advances; 2012. pp. 1-15.

[11] C. Loh, P. Lin, N. Chung, Experimental verification of building control using active bracing system, Earthquake Eng Struct Dyn 28 (1999) 1099-1119.

[12] A. Preumont, A. Seto, Active control of structures, 2008, John Wiley &

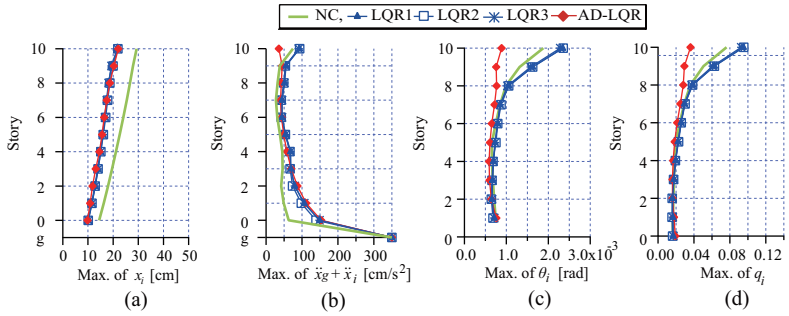

Fig. C.33: Comparison of time responses between LQRs 1-3 and AD-LQR for T_0 = 6.0 s for El-Centro wave.

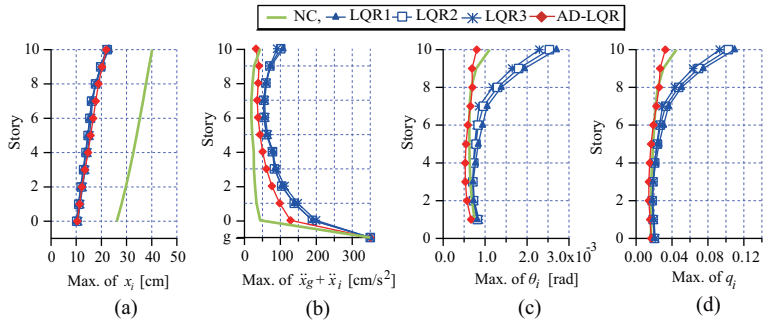

Fig. C.34: Comparison of time responses between LQRs 1-3 and AD-LQR for T_0 = 8.0 s for El-Centro wave.

Table C.9: Maximums of responses for Tokachi wave (T_0 = 6.0 s).

	Story	0	1	2	3	4	5	6	7	8	9	10
x [cm]	NC	12.6	14.1	15.5	16.5	17.3	18.0	19.8	22.2	24.9	27.9	31.2
	AD-LQR	10.9	11.7	12.3	12.9	13.5	14.1	14.7	15.2	15.8	16.6	17.8
	LQR 1	10.2	11.5	12.5	13.3	13.8	14.0	15.5	17.1	19.4	23.2	28.6
	LQR 2	9.8	11.1	12.1	12.9	13.4	14.0	15.6	17.1	19.3	22.9	28.1
	LQR 3	10.6	11.9	12.9	13.6	14.1	14.2	15.5	17.3	19.7	23.8	29.6
$\ddot{x} + \ddot{x}_g$ [cm/s^2]	NC	50.7	51.2	49.0	45.9	41.2	33.6	25.0	23.0	35.4	63.0	91.1
	AD-LQR	93.8	54.9	42.9	34.5	29.3	26.2	25.7	27.4	32.9	39.8	37.7
	LQR 1	106.3	69.3	57.0	50.6	45.0	44.3	34.9	33.3	41.4	59.9	89.2
	LQR 2	106.0	68.5	56.1	49.8	44.2	42.5	33.8	33.4	41.4	58.2	85.5
	LQR 3	100.1	66.2	57.0	52.2	46.9	44.3	34.2	32.3	40.7	64.3	95.1
θ [rad] ($\times 10^{-3}$)	NC	—	0.63	0.61	0.69	0.76	0.95	1.21	1.48	1.77	2.05	2.30
	AD-LQR	—	0.50	0.46	0.47	0.51	0.58	0.66	0.76	0.85	0.91	0.95
	LQR 1	—	0.65	0.64	0.68	0.74	0.94	1.17	1.42	1.69	1.95	2.25
	LQR 2	—	0.65	0.64	0.68	0.74	0.91	1.13	1.38	1.63	1.87	2.16
	LQR 3	—	0.63	0.63	0.68	0.77	1.00	1.25	1.52	1.81	2.09	2.40
q ($\times 10^{-2}$)	NC	1.44	1.41	1.49	1.80	2.15	2.88	3.91	5.10	6.43	7.86	9.29
	AD-LQR	1.09	1.15	1.15	1.26	1.46	1.77	2.15	2.61	3.10	3.49	3.85
	LQR 1	1.37	1.48	1.58	1.80	2.11	2.85	3.78	4.88	6.14	7.47	9.11
	LQR 2	1.37	1.47	1.58	1.80	2.10	2.77	3.66	4.72	5.93	7.19	8.72
	LQR 3	1.43	1.43	1.55	1.79	2.19	3.03	4.03	5.23	6.59	8.03	9.71

Sons, Inc., 2008

[13] K. Miyamoto, J. She, J. Imani, X. Xin, D. Sato, Equivalent-input-disturbance approach to active structural control for seismically excited buildings, Eng Struct 125 (2016) 392-399.

[14] C. Ng, Y. Xu, Semi-active control of a building complex with variable friction dampers, Eng Struct 29 (2007) 1209-1225.

[15] A. Yanik, U. Aldemir, M. Bakioglu, A new active control performance index for vibration control of three-dimensional structures, Eng Struct 62-63 (2014) 53-64.

[16] U. Aldemir, A. Yanik, B. Mehmet, Control of structural response under earthquake excitation, Comput-Aid Civil Infrastruct Eng 27 (2012) 620-638.

[17] J.P. Lynch, Y. Wang, R.A. Swartz, K.C. Lu, C.H. Loh, Implementation of a closed-loop structural control system using wireless sensor networks, Struct Control Health Monitor 15 (2007) 518-539.

[18] N. Miura, M. Kohiyama, Design method of a quadratic cost function for vibration control to maintain functions of a building during an earthquake, J Struct Constr Eng 78 (687) (2014) 923-929, in Japanese.

[19] F. Sadek and B. Mohraz, Semiactive control algorithms for structures with variable dampers, J Eng Mech 134 (9) (1998) 981-990.

[20] Y. She, T.C. Becker, S. Furukawa, E. Sato, M. Nakashima, LQR control with frequency-dependent scheduled gain for a semi-active floor isolation system, Earthquake Eng Struct Dyn 43 (2014) 1256-1284.

[21] T. Fujii, H. Fujitani, Y. Mukai, Performance evaluation of semi-active optimal control system by MR damper, J Struct Constr Eng 689 (78) (2013) 1237-1245, in Japanese.

[22] D. Sato, K. Kasai, T. Tamura, Influence of frequency sensitivity of viscoelastic damper on wind-induced response, J Struct Constr Eng 635 (74)

Table C.10: Maximums of responses for Tokachi wave (T_0 = 8.0 s).

	Story	0	1	2	3	4	5	6	7	8	9	10
x [cm]	NC	21.8	23.3	24.8	26.1	27.2	28.2	29.1	30.3	32.0	34.0	36.3
	AD-LQR	11.3	12.0	12.6	13.2	13.8	14.4	15.0	15.5	16.1	16.8	18.0
	LQR 1	12.5	13.2	14.1	14.7	14.9	14.8	14.4	16.3	19.3	23.8	29.9
	LQR 2	10.3	11.3	12.3	13.1	13.6	14.0	14.2	15.9	18.2	21.3	25.5
	LQR 3	11.3	12.1	13.0	13.7	14.2	14.3	14.3	16.1	18.7	22.4	27.7
$\ddot{x} + \ddot{x_g}$ [cm/s^2]	NC	33.5	35.3	34.4	31.0	26.2	20.7	18.3	18.2	26.2	41.3	58.8
	AD-LQR	79.8	48.8	38.3	30.9	26.2	23.5	22.9	24.4	29.4	35.8	34.1
	LQR 1	137.0	87.8	72.2	65.1	59.1	57.2	44.3	36.3	46.9	67.5	100.9
	LQR 2	139.0	85.3	68.9	62.3	56.9	50.0	42.1	37.4	44.0	55.7	79.8
	LQR 3	135.1	85.7	70.2	63.3	57.4	52.8	42.2	36.5	44.3	60.1	88.9
θ [rad] ($\times 10^{-3}$)	NC	—	0.63	0.60	0.62	0.70	0.77	0.87	1.01	1.15	1.32	1.49
	AD-LQR	—	0.43	0.40	0.41	0.45	0.51	0.59	0.68	0.76	0.81	0.86
	LQR 1	—	0.77	0.74	0.76	0.84	1.04	1.30	1.56	1.87	2.16	2.54
	LQR 2	—	0.76	0.72	0.72	0.76	0.82	0.94	1.13	1.33	1.51	2.01
	LQR 3	—	0.76	0.73	0.74	0.79	0.92	1.14	1.37	1.63	1.87	2.24
q ($\times 10^{-2}$)	NC	1.39	1.40	1.45	1.64	1.97	2.33	2.82	3.45	4.17	5.06	6.00
	AD-LQR	0.95	0.99	1.00	1.10	1.29	1.56	1.92	2.34	2.78	3.13	3.48
	LQR 1	1.64	1.76	1.83	2.01	2.38	3.16	4.22	5.36	6.80	8.27	10.3
	LQR 2	1.63	1.74	1.78	1.92	2.16	2.50	3.02	3.87	4.83	5.78	8.15
	LQR 3	1.62	1.74	1.80	1.97	2.24	2.79	3.70	4.69	5.93	7.17	9.07

Table C.11: Maximums of responses for El-Centro wave (T_0 = 6.0 s).

	Story	0	1	2	3	4	5	6	7	8	9	10
x [cm]	NC	14.4	16.3	18.0	19.6	21.1	22.6	24.0	25.4	26.7	27.9	29.3
	AD-LQR	9.8	10.8	11.8	13.1	14.5	15.6	16.4	17.5	18.7	20.3	22.1
	LQR 1	10.0	11.4	12.7	13.8	14.8	15.8	16.6	17.4	18.1	19.4	21.7
	LQR 2	10.1	11.6	12.9	14.0	15.0	16.0	16.8	17.5	18.2	19.3	21.7
	LQR 3	10.1	11.6	12.9	14.0	15.1	16.1	17.0	17.8	18.7	20.0	21.9
$\ddot{x} + \ddot{x_g}$ [cm/s^2]	NC	62.9	49.0	42.1	45.9	45.3	38.7	31.2	27.4	32.2	38.4	74.8
	AD-LQR	153.2	111.6	87.2	69.9	57.7	48.9	42.7	39.9	42.5	44.9	35.3
	LQR 1	148.9	106.0	79.6	69.0	68.1	54.5	44.3	44.5	51.2	55.5	93.0
	LQR 2	148.5	106.1	79.8	68.0	67.2	53.7	44.3	44.4	51.1	54.0	90.8
	LQR 3	138.8	98.1	73.6	66.9	66.4	53.6	41.9	42.0	48.9	53.7	93.6
θ [rad] ($\times 10^{-3}$)	NC	—	0.74	0.71	0.68	0.65	0.66	0.75	0.85	0.99	1.32	1.88
	AD-LQR	—	0.76	0.64	0.60	0.59	0.61	0.65	0.72	0.77	0.76	0.89
	LQR 1	—	0.71	0.66	0.67	0.69	0.73	0.79	0.85	1.06	1.63	2.34
	LQR 2	—	0.71	0.66	0.67	0.69	0.73	0.79	0.85	1.02	1.58	2.29
	LQR 3	—	0.68	0.64	0.66	0.68	0.75	0.79	0.87	1.06	1.63	2.35
q ($\times 10^{-2}$)	NC	1.63	1.65	1.71	1.78	1.84	1.99	2.42	2.92	3.60	5.06	7.63
	AD-LQR	1.92	1.78	1.61	1.60	1.69	1.86	2.13	2.48	2.82	2.93	3.61
	LQR 1	1.69	1.63	1.61	1.76	1.96	2.23	2.57	2.94	3.86	6.26	9.49
	LQR 2	1.70	1.64	1.61	1.76	1.96	2.23	2.57	2.94	3.74	6.09	9.27
	LQR 3	1.61	1.57	1.57	1.73	1.94	2.28	2.58	3.01	3.85	6.26	9.55

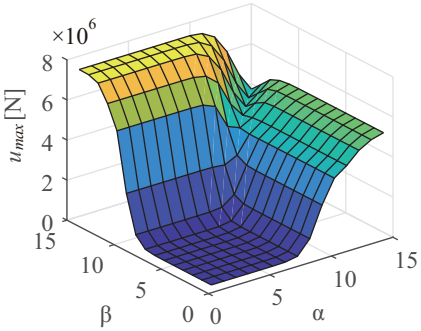

Fig. C.35: Relationship between α and β, and maximum control input for Tokachi wave (T_u = 5.0 s and T_0 = 8.0 s.

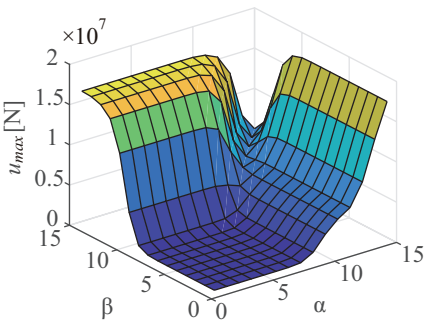

Fig. C.36: Relationship between α and β, and maximum control input for El-Centro wave (T_u = 5.0 s and T_0 = 8.0 s.

Table C.12: Maximums of responses for El-Centro wave (T_0 = 8.0 s).

	Story	0	1	2	3	4	5	6	7	8	9	10
x [cm]	NC	26.1	28.0	29.7	31.3	32.7	34.0	35.3	36.5	37.7	38.9	40.2
	AD-LQR	10.4	11.3	12.3	13.4	14.7	15.7	16.7	17.7	18.8	20.3	21.9
	LQR 1	10.0	10.8	11.7	12.7	13.7	14.5	15.3	16.1	17.9	20. 1	22.9
	LQR 2	10.7	11.6	12.6	13.5	14.5	15.3	15.9	16.5	17.8	19.6	22.0
	LQR 3	10.2	11.0	12.0	13.0	13.9	14.7	15.4	16.1	17.7	19.7	22.3
$\ddot{x} + \ddot{x_g}$ [cm/s^2]	NC	43.6	33.6	29.2	26.1	25.8	21.8	19.3	19.2	22.3	27.0	44.0
	AD-LQR	128.1	98.0	76.3	61.1	50.6	43.1	37.8	35.6	38.2	40.7	32.0
	LQR 1	189.5	138.2	103.5	84.1	80.7	61.8	54.3	53.3	59.3	73.7	107.4
	LQR 2	199.1	148.2	111.5	89.5	76.5	64.7	57.8	56.2	61.4	70.6	91.2
	LQR 3	189.1	138.5	103.8	83.3	78.1	60.7	54.5	53.5	59.4	70.8	100.7
θ [rad] ($\times 10^{-3}$)	NC	—	0.75	0.69	0.65	0.63	0.63	0.63	0.63	0.67	0.79	1.11
	AD-LQR	—	0.67	0.57	0.53	0.53	0.55	0.59	0.65	0.70	0.69	0.80
	LQR 1	—	0.82	0.72	0.71	0.77	0.84	0.94	1.05	1.38	1.94	2.70
	LQR 2	—	0.85	0.74	0.72	0.72	0.75	0.80	0.86	1.18	1.65	2.29
	LQR 3	—	0.81	0.72	0.71	0.73	0.78	0.83	0.96	1.30	1.80	2.53
q ($\times 10^{-2}$)	NC	1.66	1.66	1.66	1.70	1.78	1.89	2.02	2.15	2.43	3.03	4.49
	AD-LQR	1.68	1.56	1.42	1.42	1.51	1.67	1.92	2.25	2.56	2.66	3.26
	LQR 1	2.02	1.90	1.79	1.89	2.18	2.54	3.05	3.62	5.05	7.47	11.0
	LQR 2	2.14	1.99	1.85	1.91	2.07	2.30	2.61	2.95	4.32	6.36	9.31
	LQR 3	2.02	1.90	1.79	1.88	2.07	2.38	2.70	3.29	4.73	6.95	10.3

(2009) 75-82, in Japanese.
[23] W.S. Levine, The control handbook, 2nd ed., CRC Press, 2010.
[24] Y. Tanaka, N. Fukuwa, J. Tobita, M. Mori, Development and analysis of database for base-isolated building in Japan, J Technol Des 17 (35) (2011) 79-84, in Japanese.
[25] H. Li, J. Ou, A design approach for semi-active and smart base-isolated buildings, Struct Control Health Monitor 13 (2006) 660-681.
[26] K. Matsuda, K. Kasai, Study on dynamic behavior of high-rise base-isolated building based on its responses recorded during the 2011 Tohoku-oki earthquake, J Struct Constr Eng 704 (79) (2014) 1445-1455, in Japanese.
[27] K. Zhou, C.J. Doyle, Essentials of robust control, Prentice Hall, 1997.
[28] L.S. William S. The control handbook, CRC Press, 1995.
[29] K.W. Gawronski, Advanced structural dynamics and active control of structures, Springer, 2004.